Reduced C9orf72 function leads to defective synaptic vesicle release and neuromuscular dysfunction in zebrafish

Zoe Butti
INRS- Centre Armand-Frappier Santé et Biotechnologie
Jean Giacomotto
Queensland Brain Institute, University of Queensland
Kessen (Shunmoogum) Patten (Kessen.patten@iaf.inrs.ca)
INRS

Article

Keywords: ALS, C9orf72, synapses, motor neuron, zebrafish

Posted Date: August 7th, 2020

DOI: https://doi.org/10.21203/rs.3.rs-49118/v1

Version of Record: A version of this preprint was published at Communications Biology on June 25th, 2021. See the published version at https://doi.org/10.1038/s42003-021-02302-y.

Abstract

A hexanucleotide repeat expansion within the C9orf72 gene is the most common genetic cause of amyotrophic lateral sclerosis (ALS) and fronto-temporal dementia (FTD). Reduced levels of C9orf72 mRNA and protein have been found in ALS/FTD patients, but the role of this protein in disease pathogenesis is still poorly understood. Here, we report the generation and characterization of a stable C9orf72 loss-of-function (LOF) model in the zebrafish. We show that reduced C9orf72 function leads to motor defects, muscle atrophy, motor neuron loss and mortality in early larval and adult stages. Analysis of the structure and function of the neuromuscular junctions (NMJs) of the larvae, reveal a significant reduction in the number of presynaptic and postsynaptic structures and an impaired release of quantal synaptic vesicles at the NMJ. Strikingly, we demonstrate a downregulation of SV2a upon C9orf72-LOF and a reduced rate of synaptic vesicle cycling. Furthermore, we show a reduced number and size of Rab3a-postive synaptic puncta at NMJs. Altogether, these results reveal a key function for C9orf72 in the control of presynaptic vesicle trafficking and release at the zebrafish larval NMJ. Our study demonstrates a novel role for C9orf72 in ALS/FTD pathogenesis, where it regulates synaptic vesicle release and neuromuscular functions.

Introduction

Amyotrophic lateral sclerosis (ALS) is a progressive and ultimately lethal neuromuscular disease involving the degeneration and loss of motor neurons. Current FDA-approved treatments for ALS are only modestly effective and the disease still results in complete paralysis and death within the five first years after diagnosis. GGGGCC hexanucleotide repeat expansions within the first intron of C9or72 is the most common genetic cause of ALS and frontotemporal dementia (FTD)[1,2]. The pathogenic mechanism by which the repeat expansions cause disease may involve toxic gain-of-function (GOF) mechanisms, such as RNA toxicity [3] and protein toxicity by aberrant dipeptide repeat protein (DPR) accumulation [4,5]. Alternatively, reduced C9orf72 mRNA and protein levels in a range of patient tissues and patient-derived cell lines [1,6,7] suggest loss-of-function (LOF) by C9orf72 haploinsufficiency may also contribute to C9orf72 ALS/FTD.

The two GOF pathogenic mechanisms are extensively studied [8], while the role of C9orf72-LOF in ALS pathogenesis remains poorly understood. Importantly, in general, how the GGGGCC hexanucleotide repeat expansions cause neurodegeneration in ALS and FTD is still uncertain. The C9orf72 protein has been shown to function in a complex with the WDR41 and SMCR proteins as a GEF for Rab8 and Rab39 [9,10]. It has also been proposed to play a role in autophagic flux[9,11,12], endosomal trafficking [13–15] and regulating AMPA receptor levels [16].

Synaptic alterations at neuromuscular junctions (NMJs) have been found in ALS patients and in animal models of ALS. For instance, Killian et al observed that initial compound motor action potentials (CMAP) in ALS patients were of low amplitude but did not demonstrate early post-exercise facilitation (reduction in decrement occurred at 3 minutes post-exercise). The low baseline CMAP amplitudes with decrement

may suggest a pre-synaptic transmission deficit [17]. I*n vitro* microelectrode studies of ALS patient anconeus muscle demonstrated reduced pre-synaptic acetylcholine quantal stores, possibly explained by the diminished size of nerve terminals [17]. In mutant *SOD1*-expressing mice [18,19] an early retraction of presynaptic motor endings was observed long before the death of motoneurons [20]. Such an observation was also observed in tissue from patients with ALS [21]. In zebrafish, expression of mutant human TARDBP^{G348C} mRNA or *FUS*^{R521H} resulted in impaired transmission, reduced frequency of miniature endplate currents (mEPCs) and reduced quantal transmission at the NMJ [22,23]. C9orf72 is expressed presynaptically and postsynaptically [16]. The function of C9orf72 at synapses remains an interesting and largely unexplored, yet a full understanding of its synaptic function can extend its contribution to ALS pathogenesis and uncover therapeutic targets.

Zebrafish is a powerful tool for studying neurological diseases relevant to humans including ALS [24]. Using a stable transgenic zebrafish model with reduced C9orf72 expression, we analyzed the effects of reduced C9orf72 function on the zebrafish's neuromuscular system. These zebrafish display behavioural deficits and early mortality observed in C9orf72-ALS patients. C9orf72 silencing resulted in impaired synaptic activity and downregulation of the synaptic protein, SV2a. Our findings suggest that loss-of-function mechanisms underlie defects in synaptic function in ALS.

Results

Generation of stable C9orf72-LOF model in zebrafish

To better understand the role of *C9orf72*-LOF in ALS/FTD pathogenesis, we generated a stable transgenic zebrafish gene-silencing model. A single conserved *C9ORF72* ortholog is present in zebrafish on its chromosome 13. To achieve transgenic *c9orf72* gene silencing in zebrafish, we used a recent miRNA-based gene-silencing approach developed for zebrafish [25]. Unlike morpholino-based knockdown approach, transgenic zebrafish lines that have been constructed to stably express miRNAs designed to target knockdown desired genes of interest have no apparent non-specific toxic effects [26]. The miRNA knockdown technique consists in the use of transgenic DNA construct allowing the expression of synthetic miRNA targeting the 3' UTR of a gene-of-interest, here the endogenous zebrafish *c9orf72* (Fig. 1a). As presented more in details in the method section, we designed 4x different miRNAs targeting specifically *c9orf72* (C9orf72-miR) that we inserted downstream of a dsRED marker and under the control of a ubiquitous promoter (Ubiquitin), the overall sequence was recombined into a mini-Tol2-R4R2 destination plasmid. To generate a transgenic line, this Tol2-DNA construct was co-injected with transposase mRNA in fertilized eggs at one-cell stage for enhanced genomic integration of the DNA construct [27]. To ease the selection of the founders/carriers, we also included an eGFP cassette under the crystallin promoter (Fig. 1b). Founders with eyes displaying GFP fluorescence were selected and raised to generate a stable and heritable C9orf72-miR LOF line (hereafter referred as C9-miR). F1 transgenic fish gave a birth to a ratio of close to 50% positive GFP embryos when outcrossed with wild-type animals, suggesting the presence of a single genomic insertion.

We first analysed *C9orf72* silencing efficiency in our C9-miR line by RT-qPCR and western blotting. We showed a significant decrease in the level of C9orf72 *mRNA* (Fig. 1c) associated with a 50% decrease of C9orf72 protein (Fig. 1d, e). Altogether, these results indicate that our genetic approach efficiently reduces the C9orf72 protein levels *in vivo* and this C9-miR line can be used to understand the role of C9orf72 haploinsufficiency in ALS.

C9orf72-LOF model shows early motor behavioural defects and reduced viability

We did not observe any overt morphological abnormalities during embryonic development (0–5 dpf) in C9-miR fish (Fig. 2a). From 6–14 dpf, C9-miR larvae exhibited gradual morphological defects such as an unusual body curve and premature death (Fig. 2b,c). C9orf72 partial depletion importantly led to a significant decrease in survival at 10 dpf compared to wild-type controls; with a survival rate of 2–5% after 15 dpf (Fig. 2b).

We, next, examined whether normal zebrafish motor behaviour was affected in larval C9-miR zebrafish (4–11 dpf). To assess motor activity, larval zebrafish that did not display any of the abnormal morphological defects were selected and monitored using the automated Noldus Ethovision XT behaviour monitoring system. A significant decrease in motor activity was observed in C9-miR fish as compared to controls, as of 6 dpf (Fig. 2c,d). Such an impaired motor behaviour early on in C9-miR zebrafish is consistent with findings that we and others have reported in several other zebrafish models of ALS [24,28–30].

C9orf72-LOF zebrafish model display adult hallmark features of ALS

C9-miR fish that survive past 15 dpf were also studied at adult stages for hallmarks of ALS such as muscle atrophy, motoneuron death and paralysis. Hematoxylin & eosin (H&E) staining of cross-section of fish body trunk revealed that muscle in adult C9-miR exhibited severe atrophy (Fig. 3a), with a significant reduction in the thickness of the fibres (Fig. 3b). Choline acetyltransferase (ChAT) staining is a hallmark feature of cholinergic motor neurons. ChAT immunostaining was performed on the spinal cord sections of adult C9-miR fish and the mature motor neurons in the C9-miR fish were reduced in size by 19.2 ± 0.02 % (Fig. 3c). At the motor behavioural level, we observed an impaired swimming ability in C9-miR compared to controls (Fig. 3d, Supplemental Videos). Prior to death, C9-miR fish spent their time in the bottom of the tank with weak movements. Adult survival was also monitored and we observed that by 16 months post-fertilisation, more than 80-90% of the adult C9-miR zebrafish die.

Cytoplasmic aggregation of Trans-activation response element (TAR) DNA-binding protein 43 (TDP-43) is a major pathological hallmark of ALS [31]. TDP-43 form aggregates in neurons, glial cells [31] and axial skeletal muscle [32]. By taking advantage of the relatively large nucleus and cytoplasm of skeletal muscle cells, we examined whether TDP-43 pathology exist in our model. Using a specific antibody that recognizes the highly homologous human TDP-43 ortholog in zebrafish [33], we showed that this protein is localized to the nucleus of the skeletal muscle cells in wild-type zebrafish (Fig. 4a). In contrast, in C9-miR zebrafish, we observed clusters of TDP-43 in skeletal muscles (Fig. 4b). We then analyzed these clusters

further to examine their precise cellular localization and found that they are predominantly located outside of the nucleus. Altogether, our findings provide strong evidences that C9orf72 silencing in zebrafish recapitulates key pathological hallmarks of ALS.

C9orf72 silencing affects NMJ structural integrity and quantal release

We next examined NMJ integrity by performing double-immunohistochemistry on fixed embryos using specific presynaptic (SV2) and postsynaptic markers (a-bungarotoxin). Analysis revealed no change the primary motor neuron axon architecture and in colocalization of pre- and post-synaptic signals in C9-miR fish at 2 dpf (Fig. 5a,b) and 4 dpf. However, in 6 dpf C9-miR larvae, we observed a significant reduction in the number of colocalizing pre- and post- synaptic puncta (Fig. 5c,d). These results indicate that, while the synaptic structures of the NMJ develop properly and are preserved at early embryonic stages in C9-miR, they do start to degenerate from 6 dpf.

To investigate if alterations in NMJ integrity had functional consequences on synaptic transmission in the 6 dpf C9-miR larvae, we recorded and analysed the spontaneous miniature end plate currents (mEPCs) that occur naturally and spontaneously at synapses and represent the unitary event during synaptic transmission (Fig. 6a). We observed that the frequency of mEPCs in C9-miR was significantly reduced compared to controls (Fig. 6b), suggesting a reduction in the number of functional presynaptic endings. The mean amplitude of mEPCs was also found to be smaller in zebrafish C9-miR compared to wild-type zebrafish (Fig. 6c). We observed that the mEPCs from the muscle of C9-miR larvae and controls shared similar rise time and decay time constant kinetics (Fig. 6d).

C9orf72 regulates synaptic vesicle exocytosis and synapse stability at the NMJ

To gain more insights into molecular processes and pathways affected, we determined global changes at the proteomic levels by isolating total proteins at 6 dpf from C9-miR and wild-type siblings. We identified a total of 2602 proteins that were covered by two or more uniques peptides and were quantifiable in four biological replicates (FDR≤1%). Most of the proteins in wild-type and C9-miR were at comparable expression levels. Only 24 proteins were found to be dysregulated ($p<0.05$; Table S2). Of these hits, 12 were upregulated and 12 were downregulated in C9-miR fish (Fig. 7a). These differentially expressed proteins (DEPs) were classified into functional clusters according to the PANTHER classification system (Fig. 7b-e). The classification results revealed that many DEPs were distributed into six protein classes (Fig. 7b). These proteins are classified in three molecular functions namely binding (20%), structural molecule activity (20%) and catalytic activity (60%) (Fig. 7c). They are involved in biological processes, being cellular process, metabolic process and biological regulations the most represented ones with 38%, 23.1% and 15.4% of proteins respectively (Fig. 7d). Cellular component analysis revealed that the DEPs belong in majority to the organelle, membrane and synapse categories (Fig. 7e). Consistent with the synaptic dysfunction phenotype, we identified a strong downregulation of synaptic proteins (Fig. 7a; Table S2). Among these proteins, the top hit of dysregulated proteins is the synaptic protein, synaptic vesicle-associated protein 2a (SV2a). Importantly, a recent study showed that SV2a is reduced in C9orf72-

ALS patient-derived IPS neurons [34]. This data links the findings in our C9orf72 loss-of-function model to ALS.

Given that SV2a is an essential component of active zones and synaptic release machinery, we next sought to further assess synaptic activity at the NMJ by measuring synaptic vesicle (SV) cycling at the NMJ in zebrafish larvae using the fluorescent styryl dye, FM1-43 [35,36]. C9-miR and controls larvae were exposed to FM1-43 and its uptake into NMJ presynaptic boutons was monitored. The presynaptic terminals were acutely depolarized with a high [K+] HBSS solution (45 mM) to drive the exocytotic activity, SV cycle and load FM1-43 and label synaptic clusters. In controls, we observed strong fluorescence staining along terminal axon branches at individual synaptic varicosity boutons (Fig. 8a). While in C9-miR fish we found a significant reduction in FM1-43 loading in presynaptic terminals (Fig. 8b), indicating slowing of the exocytotic activity and the overall SV cycle. These findings reveal a key role for C9orf72 in regulating presynaptic vesicle release at NMJ.

To assess organization of the presynaptic structure at NMJ, we examined the expression of Rab3a, a protein associated with vesicles at active zones that is essential for synaptic vesicle release and neurotransmission (Fig. 8c-e). We found a reduced number of Rab3+ puncta in C9-miR fish compared to controls (Fig. 8c-d) as well as the area of the putative synapses were smaller in C9-miR fish (Fig. 8e).

Discussion

Despite advances in studies of C9orf72-ALS, understanding the function of C9orf72 remains a key research element that is poorly explored. We generated a *C9orf72*-related ALS stable zebrafish line with a reduced expression of C9orf72. These fish display motor defects, muscle atrophy, motor neuron loss and mortality in early larval and adult stages. Additionally, they exhibit TDP-43 pathology, which is a key hallmark of ALS. Analysis of the structure and function of the NMJs, revealed a significant reduction in the number of presynaptic and postsynaptic structures and an impaired release of quantal synaptic vesicles at the NMJ in the C9-miR line. We also identified a novel role of C9orf72 in controlling presynaptic vesicle trafficking and release at the zebrafish larval NMJ.

Reduced C9orf72 mRNA and protein levels in a range of patient tissues and patient-derived cell lines [1,6,7]. Our C9orf72 zebrafish model provides support to a loss-of-function mechanism underlying *C9orf72-dependant* ALS. Our data are consistent with deletion or transient knockdown models in *C. elegans* [37] and zebrafish [38] respectively, showing defective motor phenotypes. However, in contrast, no motor neurons deficits were reported in *C9orf72* knock-out mice [39–41]. In addition, these mice also did not exhibit TDP-43 proteinopathy. The model presented here, importantly, display TDP-43 pathology and replicates haploinsufficiency as a major contributor to *C9orf72* ALS rather than a full ablation of C9or72 loss-of-function model. Intriguingly, the motor phenotypes observed in C9-miR zebrafish are consistent with several other zebrafish ALS models, including zebrafish model expressing C9orf72-related repeat expansions or DPR [28,42,43]. However, the presence a reduced level of C9orf72 mRNA or protein in these models, as in ALS/FTD, was not examined in these studies. Of note, the expression of GGGGCC repeat

expansions or DPR in zebrafish are toxic [42,44,45], consistent with several studies in neurons and other animals. We found that expression of GGGGCC repeat expansions in our C9-miR exacerbated toxicity and resulted in death of zebrafish by 6 dpf (Figure S1). Such a synergistic interplay between reduced C9orf72 function and repeat-dependent gain of toxicity was observed in a recent study by Zhu and colleagues [46].

An important finding of this study is the synaptic impairments in C9-miR fish. The reduced frequencies and amplitudes of quantal neurotransmission events are consistent with observations made in several non-C9orf72 ALS models [22,23] and in tissue from patients with ALS [21]. We also report significant reductions in synaptic vesicle exocytosis and number and area putative synaptic puncta at NMJs. Additionally, we show a decrease in the expression of synaptic vesicle protein SV2a. These findings provide a novel role of C9orf72 in synaptic physiology at the presynaptic level. Interestingly, consistent with our findings, SV2a was also recently found at reduce levels in C9orf72-ALS patient-derived IPS neurons [34]. Ablation of SV2a function in knockout models resulted in reduced number of readily releasable pool of synaptic vesicles, diminished release probability and reduction in spontaneous synaptic events [47,48]. Whether C9orf72 directly or indirectly regulates the level of SV2a in presynaptic compartments remains to be investigated. Intriguingly, similar observations of loss of SV2a and synaptic dysfunction were also observed in neurons expressing the C9orf72-related glycine-alanine (GA) DPR [34]. DPR proteins can disrupt pre-mRNA splicing in ALS/FTD patients [49]. It is possible that the expression of GA DPR in neurons reduce the level of *C9orf72* transcripts leading to the synaptic phenotypes.

Rab3a is important for transport of synaptic vesicles and their docking at active zones [50]. It regulates synaptic transmission and it is associated with synaptic vesicles through GEF activity [51,52]. For instance, at rab3a-deficient terminals in mice, synaptic secretion response recovered slowly and incompletely following exhaustive stimulation [50]. In addition, the replenshiment of docked vesicles following exhaustive stimulation at these terminals was also impaired [50]. DENN domain containing proteins such as C9orf72 can function as Rab GEFs, enabling their activation, recruitment and interaction with downstream effectors [53,54]. A previous study had identified Rab3a as part of complex interacting with C9orf72 [7]. It is plausible that in addition to the effect of reduced SV2a on synaptic dysfunction, synaptic vesicle exocytosis and quantal transmission defects in C9-miR maybe exacerbated due to the altered function of C9orf72 as a GEF for Rab3a and its recruitment to synaptic vesicles.

In conclusion, we generated a stable C9orf72 LOF model in zebrafish that recapitulated some major hallmarks of ALS and enhanced our understanding of ALS pathogenesis. Importantly, our findings demonstrate that loss of C9orf72 function impairs synaptic function at NMJs and result in motor deficits. We postulate that synaptic deficits observed in repeat expansions or DPR models maybe the result of an indirect effect related to an impact of the repeats on C9orf72 levels.

Methods

Zebrafish Husbandry

Adult zebrafish (*Danio rerio*) were maintained at 28 °C at a light/dark cycle of 12/12 h in accordance with Westerfield zebrafish book[55]. Embryos were raised at 28.5 °C, and collected and staged as previously described[56]. All experiments were performed in compliance with the guidelines of the Canadian Council for Animal Care and the local ethics committee.

Anti-c9orf72 (synthetic miRNA) RNAi target site selection

We first generated a template with c9orf72 RNA sequence, including 5'- and 3'-UTR sequence. 3'-UTR minimal sequence has been obtained from analysis of data available on ensembl (http://asia.ensembl.org/) with zebrafish GRCz11 genome iteration and on Targetscan Fish website (http://www.targetscan.org/fish_62/). We analysed and annotated *c9orf72* sequence for identifying and avoiding selecting target sequence that would run across i) potential polymorphisms in the 3'UTR sequence and ii) endogeneous miRNA. Based on these data we selected 4x unique target sites on the 3'UTR sequence of *c9orf72* that do not show any off-specific match across the zebrafish genome. Each site and corresponding mature anti-*c9orf72* synthetic miRNA are presented in Table S1.

RNAi Plasmid generation

To generate the *c9orf72*-RNAi transgene (Tol2-UBI:dsRED:*c9rof72*-1234-Cryst:eGFP) used in this study to silence the gene *c9orf72*, we first used a previously generated empty RNAi-plasmid compatible with the tol2-kit, pME-RNAi642 (PMID 26051838). Based on this design and following previous instructions, we designed 4x anti-*c9orf072* miRNAs stem loops compatible with the pME-RNAi642 (Table S1). pME-RNAi642 was digested with BsmBI and gel-extracted. Each stem loops (x4) were annealed and inserted into pME-RNAi642 following previous instructions (PMID 26051838). 4x different pME-RNAi-*c9orf72* has been generated and named pME-RNAi-*c9orf72*-1 to -4. We further chained the 4x stem loop. We ended with a 4x-anti-*c9orf72* RNAi pME plasmid named pME-RNAi-*c9orf72*-1234. In parallel, a custom made 1456-pDEST-miniTol2-R4-R2_Cryst:eGFP clone was generated; this clone presents miniTol2 sequence surrounding gateway Att-R4 and Att-R2 sequences followed by a Cryst:eGFP cassette (Crystallin-promoter driving eGFP into lenses for identifying transgenic/carrier fish). Following manufacturer instruction, we performed a Gateway LR-reaction mixing/recombining p5E-Ubi (Ubiquitin promoter) and pME-RNAi-*c9orf72*-1234 into 1456-pDEST-miniTol2-R4-R2_Cryst:eGFP. Final plasmid obtain was named Tol2-UBI:dsRED:*c9rof72*-1234-Cryst:eGFP and used to perform one-cell stage injections for transgene integration.

Injections for transgene integration

To integrate Tol2-UBI:dsRED:*c9orf72*-1234-Cryst:eGFP construct into the zebrafish genome, 1 nl of a mix of 30 ng/µl of construct and 25 ng/µl of Transposase mRNA was injected into one-cell stage embryos using the Picospritzer III pressure ejector.

Western Blot

For each condition, thirty 6 dpf fish were lysed in 150 µL RIPA buffer (1% NP-40, 0,5% Na^+ desoxycholate, 0,1% SDS in PBS supplemented with proteases cocktail inhibitor) for 90 seconds on ice and left

incubated for 10 minutes still on ice. Samples were then centrifuged at 10 000 rpm for 10 minutes at 4 °C. Supernatants were collected and stored at -80 °C. 40 ng of protein and 2X Laemmli buffer (BioRad) were boiled at 95 °C for 5 minutes, loaded in a 7,5% acrylamide gel electrophoresis and blotted on a PVDF membrane using Trans-blot Turbo transfer system device (BioRad). Membrane was then probed with Novus Npb2-15656 (1:5000) antibody against C9orf72 and Sigma A5441 (1:5000) antibody was used against β-actin and revealed using Calrity Western ECL substrate (BioRad). Quantifications were performed with Image Lab (BioRad) normalizing using β-actin.

Gene expression study

RNA extraction was performed on 2 dpf larvae using Trizol reagent (Sigma). 30 larvae were selected and lysed on ice for 30 seconds with 250 µL of Trizol reagent, 250 µL of reagent were added before incubating the samples at room temperature for 5 minutes. 100 µL of Chloroform were added before vortexing the samples and incubated à RT° for 2 minutes and centrifuged for 15 minutes at 4 °C at 12000 rpm. To aqueous phase was transferred in a new tube and an equivalent volume of isopropanol was added. Samples were mixed by inversion, incubated 10 minutes at RT° and centrifuged for 10 minutes at 4 °C at 12,000 rpm. Pellet was then washed with 75% ethanol, left to dry for 5 minutes and resuspended in 10 to 30 µL of DEPC H_2O. Samples were then dosed using Nanodrop device (ThermoScientific). 1 µg of RNA from each sample was used for retro transcription performed with the superscript VILO reverse transcription mix (Invitrogen). PCR was performed on 1 µL of cDNA using BioRad mix. *Elf1a* was used as control gene expression.

GGGGCC expansion repeat microinjections

GGGGCC repeat constructs (p3s and p91s) were kindly provided by Dr. Ludo Van Den Bosch and Dr. Adrian Isaacs. Synthesis of mRNAs and microinjections were performed as previously described [43].

Survival assay

Zebrafish larvae were screened for GFP positive eyes at 2 dpf and split in 4 petri dishes of 25 fishes. Dead fishes were counted and reported everyday during 17 days. Larvae were fed starting 7 dpf and dishes were cleaned twice a day.

Behavioural assay

Zebrafish control or *C9orf72-mut* larvae were transferred individually into a 96-well plate and locomotor activity was recorded using Basler GenIcam camera and DanioVision recording chamber (Noldus). After 30 of dark exposition, fishes were exposed to light for two hours. Analysis was performed using the Ethovision XT 12 software (Noldus) to quantify the distance swam.

Immunofluorescence staining

Zebrafish at 2 and 6 dpf were fixed in 4% PFA at 4 °C, overnight, washed in PBS-Tween the next day, incubated in 1 mg mL^{-1} collagenase (for 30 minutes for 2 dpf fishes and 180 minutes for 6 dpf fishes) and collagenase was washed in PBS-Tween. Fishes were incubated in blocking solution (2% NGS, 1%

BSA, 1% DMSO, 1% Triton-X in PBS) for an hour and in α-bungarotoxin (Thermofisher T1175) for 30 minutes. After washing and blocking for an hour, fishes were incubated with primary antibody (SV2, 1:200; Rab3a, 1:100) overnight at 4 °C. Next day, fishes were washed and incubated in secondary antibody (goat anti mouse 488, 1:1000) overnight at 4 °C. Next day, fishes were washed and mounted in 80% glycerol. Slides were imaged with a Zeiss confocal microscope.

Hematoxylin & Eosin staining

For the muscle and spinal cord staining, 4 whole fishes of each genotype were fixed in 4% PFA for 72 h. Fishes were embedded in paraffin and 15 µm sections were obtained using microtome. Paraffin was removed by incubating slides in xylene twice and samples were rehydrated with 4 successive baths of respectively 100%, 95%, 70% and 50% ethanol in distilled water. Hematoxylin and eosin staining was then performed.

Motoneuron staining

Adult zebrafish body trunk was crossed-sectioned using a microtome at 15 µm thick slices. Paraffin was removed, and samples were rehydrated using same technique as described above. Samples were then rinsed in PBS several times and unmask antigen step was made using citrate buffer (1M, pH 6). Citrate was washed off with several PBS baths and incubated in 0,3% Triton-X. Samples were incubated in blocking buffer (1% DGS, 0,4% Triton-X) for an hour. Primary antibody was added at 1:500 and left overnight at 4 °C. Samples were washed on the next day in PBS, blocked again and incubated in secondary antibody at 1:750.

FM1-43 staining

Zebrafish larvae were first anesthetized in Evans solution (134 mM NaCl, 2,9 mM KCl, 2,1 mM CaCl, 1,2 $MgCl_2$, 10 mM Hepes, 10 mM glucose) containing 0,02% tricaine before being pinned on a Sylgard coated dish under the head and at the tail. Skin was then carefully removed in order to expose the muscles. Pinned fish was then exposed to Evans solution containing 10 µM of FM1-43 during 10 minutes to allow preloading penetration of the dye. Then the fish was exposed to HBSS solution with high potassium concentration (97 mM NaCl, 45 mM KCl, 1 mM $MgSO_4$, 5 mM Hepes, 5 mM $CaCl_2$. and 10 µM of FM1-43 in order to load the dye at the synaptic cleft during 5 minutes. 3 more minutes in Evans solution with 10 µM of FM1-43 finished the loading and finally, the fish was washed with a low calcium Evans solution (0,5 mM $CaCl_2$) three time for 5 minutes. The fish was then imaged using a 40X Examiner microscope (Zeiss).

Electrophysiology recordings

Muscle recordings were performed on fishes that had been previously anesthetized in an extracellular solution (134 mM NaCl, 2,9 mM KCl, 1,2 mM MgCl, 10 mM Hepes, 10 mM glucose, pH 7,8) containing 0,02% tricaine before being pinned on a Sylgard coated dish under the head and at the tail. Skin was then carefully removed in order to expose the muscles. Fish was then washed with the extracellular solution containing 1 µM of tetrodotoxine in order to avoid action potentials firing. Patch clamp electrodes (1–2

MΩ) were filled with an intracellular solution (130 mM CsCl, 8 mM NaCl, 2 mM CaCl, 10 mM Hepes, 10 mM EGTA, pH 7,4). Calcium currents were recorded in the whole-cell configuration with an Axopatch 200B patch-clamp amplifier (Molecular Devices), and series resistance was compensated by at least 85% using the amplifier's compensation circuitry. Voltage protocol generation and data acquisition were performed using the pCLAMP10 software (Molecular Devices).

Mass spectrometry sample preparation

Proteins were extracted with the protocol used for western blot protein extraction. Then, a 1:8:1 ratio was used to precipitate proteins, 1X of cell lysates, 8X of 100% ice cold acetone and 1X of 100% tricholoroacetic acid in low binding protein tubes. 20 µg of proteins were precipitated. Proteins were incubated at -20 °C for 12 hours and centrifuged at 11,500 rpm for 15 minutes at 4 °C. Supernatant was then discarded.

A standard TCA protein precipitation was first performed to remove detergents from the samples (or acetone precipitation). Protein extracts were than re-solubilized in 10 µL of a 6M urea buffer. Proteins were reduced by adding 2.5 µL of the reduction buffer (45 mM DTT, 100 mM ammonium bicarbonate) for 30 min at 37ºC, and then alkylated by adding 2.5 µL of the alkylation buffer (100 mM iodoacetamide, 100 mM ammonium bicarbonate) for 20 min at 24ºC in dark. Prior to trypsin digestion, 20 µL of water was added to reduce the urea concentration to 2M. 10 µL of the trypsin solution (5 ng/µL of trypsin sequencing grade from Promega, 50 mM ammonium bicarbonate) was added to each sample. Protein digestion was performed at 37ºC for 18 h and stopped with 5 µL of 5% formic acid. Protein digests were dried down in vacuum centrifuge and stored at -20 ºC until LC-MS/MS analysis.

Mass spectrometry (LC-MS/MS)

Prior to LC-MS/MS, protein digests were re-solubilized under agitation for 15 min in 10 µL of 0.2% formic acid. Desalting/cleanup of the digests was performed by using C18 ZipTip pipette tips (Millipore, Billerica, MA). Eluates were dried down in vacuum centrifuge and then re-solubilized under agitation for 15 min in 12 µL of 2%ACN / 1% formic acid. The LC column was a PicoFrit fused silica capillary column (15 cm x 75 µm i.d; New Objective, Woburn, MA), self-packed with C-18 reverse-phase material (Jupiter 5 µm particles, 300 Å pore size; Phenomenex, Torrance, CA) using a high pressure packing cell. This column was installed on the Easy-nLC II system (Proxeon Biosystems, Odense, Denmark) and coupled to the Q Exactive (ThermoFisher Scientific, Bremen, Germany) equipped with a Proxeon nanoelectrospray Flex ion source. The buffers used for chromatography were 0.2% formic acid (buffer A) and 100% acetonitrile/0.2% formic acid (buffer B). Peptides were loaded on-column at a flowrate of 600 nL/min and eluted with a 2 slope gradient at a flowrate of 250 nL/min. Solvent B first increased from 2 to 40% in 120 min and then from 40 to 80% B in 20 min. LC-MS/MS data was acquired using a data-dependant top17 method combined with a dynamic exclusion window of 7 sec. The mass resolution for full MS scan was set to 60,000 (at m/z 400) and lock masses were used to improve mass accuracy. The mass range was from 360 to 2000 m/z for MS scanning with a target value at 1e6, the maximum ion fill time (IT) at 100 ms, the intensity threshold at 1.0e4 and the underfill ratio at 0.5%. The data dependent MS2

scan events were acquired at a resolution of 17,500 with the maximum ion fill time at 50 ms and the target value at 1e5. The normalized collision energy used was at 27 and the capillary temperature was 250ºC. Nanospray and S-lens voltages were set to 1.3–1.7 kV and 50 V, respectively.

The peak list files were generated with Proteome Discoverer (version 2.3) using the following parameters: minimum mass set to 500 Da, maximum mass set to 6000 Da, no grouping of MS/MS spectra, precursor charge set to auto, and minimum number of fragment ions set to 5. Protein database searching was performed with Mascot 2.6 (Matrix Science) against the Refseq Danio Rerio protein database. The mass tolerances for precursor and fragment ions were set to 10 ppm and 0.1 Da, respectively. Trypsin was used as the enzyme allowing for up to 1 missed cleavage. Cysteine carbamidomethylation was specified as a fixed modification, and methionine oxidation as variable modifications. Data analysis was performed using Scaffold (version 4.8).

Statistical analysis

All zebrafish experiments were performed on at least three replicates (N) and each consisted of a sample size (n) of 5–30 fish. Data are presented as Mean ± SEM. Significance was determined using either Student's t-test or One-way ANOVA followed by multiple comparisons test. A Tukey post-hoc multiple comparisons test was used for normally distributed and equal variance data. Kruskal-Walllis ANOVA and Dunn's method of comparison were used for non-normal distributions. All graphs were plotted using the Graphpad PRISM software. Significance is indicated as * $p < 0.05$, ** $p < 0.01$ and *** $p < 0.001$.

Declarations

Conflicts of interest

The authors declare no competing interests.

Acknowledgments

This study was supported by the Society of ALS Canada (SP). SP is supported by the Natural Science and Engineering Research Council, Canadian Foundation for Innovation (CFI), Canadian Institutes of Health Research (CIHR), an ALS Canada-Brain Canada Career Transition Award and a FRQS Junior 1 research scholar. SP holds the Anna Sforza Djoukhadjian research chair in ALS. JG is supported by a NHMRC Investigator Grant (Fellowship APP1174145), a NHMRC Project Grant (APP1165850) and a Rebecca L. Cooper Medical Research Project Grant (PG2019405). The authors would like to summer student Gabrielle Fortier for her assistance in some of the zebrafish experiments.

Data Availability

Data represented in this manuscript are stored on hard-drives for permanent storage and on the cloud. These data as well as the material used in this study will be available on request.

References

1. DeJesus-Hernandez, M. *et al.* Expanded GGGGCC hexanucleotide repeat in noncoding region of C9ORF72 causes chromosome 9p-linked FTD and ALS. *Neuron* **72**, 245–256, doi:10.1016/j.neuron.2011.09.011 (2011).
2. Renton, A. E. *et al.* A hexanucleotide repeat expansion in C9ORF72 is the cause of chromosome 9p21-linked ALS-FTD. *Neuron* **72**, 257–268, doi:10.1016/j.neuron.2011.09.010 (2011).
3. Zu, T. *et al.* RAN proteins and RNA foci from antisense transcripts in C9ORF72 ALS and frontotemporal dementia. *Proceedings of the National Academy of Sciences of the United States of America* **110**, E4968-4977, doi:10.1073/pnas.1315438110 (2013).
4. Ash, P. E. *et al.* Unconventional translation of C9ORF72 GGGGCC expansion generates insoluble polypeptides specific to c9FTD/ALS. *Neuron* **77**, 639–646, doi:10.1016/j.neuron.2013.02.004 (2013).
5. 10.1007/s00401-013-1189-3
   Mori, K. *et al.* Bidirectional transcripts of the expanded C9orf72 hexanucleotide repeat are translated into aggregating dipeptide repeat proteins. *Acta neuropathologica* **126**, 881–893, doi:10.1007/s00401-013-1189-3 (2013).
6. Belzil, V. V. *et al.* Reduced C9orf72 gene expression in c9FTD/ALS is caused by histone trimethylation, an epigenetic event detectable in blood. *Acta neuropathologica* **126**, 895–905, doi:10.1007/s00401-013-1199-1 (2013).
7. Frick, P. *et al.* Novel antibodies reveal presynaptic localization of C9orf72 protein and reduced protein levels in C9orf72 mutation carriers. *Acta neuropathologica communications* **6**, 72, doi:10.1186/s40478-018-0579-0 (2018).
8. Balendra, R. & Isaacs, A. M. C9orf72-mediated ALS and FTD: multiple pathways to disease. *Nature reviews. Neurology* **14**, 544–558, doi:10.1038/s41582-018-0047-2 (2018).
9. Sullivan, P. M. *et al.* The ALS/FTLD associated protein C9orf72 associates with SMCR8 and WDR41 to regulate the autophagy-lysosome pathway. *Acta neuropathologica communications* **4**, 51, doi:10.1186/s40478-016-0324-5 (2016).
10. Corbier, C. & Sellier, C. C9ORF72 is a GDP/GTP exchange factor for Rab8 and Rab39 and regulates autophagy. *Small GTPases* **8**, 181–186, doi:10.1080/21541248.2016.1212688 (2017).
11. Ugolino, J. *et al.* Loss of C9orf72 Enhances Autophagic Activity via Deregulated mTOR and TFEB Signaling. *PLoS genetics* **12**, e1006443, doi:10.1371/journal.pgen.1006443 (2016).
12. Yang, M. *et al.* A C9ORF72/SMCR8-containing complex regulates ULK1 and plays a dual role in autophagy. *Science advances* **2**, e1601167, doi:10.1126/sciadv.1601167 (2016).
13. Sellier, C. *et al.* Loss of C9ORF72 impairs autophagy and synergizes with polyQ Ataxin-2 to induce motor neuron dysfunction and cell death. *The EMBO journal* **35**, 1276–1297,

doi:10.15252/embj.201593350 (2016).

14. Zhang, Y. *et al.* The C9orf72-interacting protein Smcr8 is a negative regulator of autoimmunity and lysosomal exocytosis. *Genes & development* **32**, 929–943, doi:10.1101/gad.313932.118 (2018).
15. Shi, Y. *et al.* Haploinsufficiency leads to neurodegeneration in C9ORF72 ALS/FTD human induced motor neurons. *Nature medicine* **24**, 313–325, doi:10.1038/nm.4490 (2018).
16. Xiao, S., McKeever, P. M., Lau, A. & Robertson, J. Synaptic localization of C9orf72 regulates post-synaptic glutamate receptor 1 levels. *Acta neuropathologica communications* **7**, 161, doi:10.1186/s40478-019-0812-5 (2019).
17. Maselli, R. A. *et al.* Neuromuscular transmission in amyotrophic lateral sclerosis. *Muscle & nerve* **16**, 1193–1203, doi:10.1002/mus.880161109 (1993).
18. Fischer, L. R. *et al.* Amyotrophic lateral sclerosis is a distal axonopathy: evidence in mice and man. *Experimental neurology* **185**, 232–240 (2004).
19. Frey, D. *et al.* Early and selective loss of neuromuscular synapse subtypes with low sprouting competence in motoneuron diseases. *The Journal of neuroscience: the official journal of the Society for Neuroscience* **20**, 2534–2542 (2000).
20. Murray, L. M., Talbot, K. & Gillingwater, T. H. Review: neuromuscular synaptic vulnerability in motor neurone disease: amyotrophic lateral sclerosis and spinal muscular atrophy. *Neuropathology and applied neurobiology* **36**, 133–156, doi:10.1111/j.1365-2990.2010.01061.x (2010).
21. Maselli, R. A. *et al.* Neuromuscular transmission in amyotrophic lateral sclerosis. *Muscle & nerve* **16**, 1193–1203, doi:10.1002/mus.880161109 (1993).
22. Armstrong, G. A. & Drapeau, P. Calcium channel agonists protect against neuromuscular dysfunction in a genetic model of TDP-43 mutation in ALS. *The Journal of neuroscience: the official journal of the Society for Neuroscience* **33**, 1741–1752, doi:10.1523/JNEUROSCI.4003-12.2013 (2013).
23. Armstrong, G. A. & Drapeau, P. Loss and gain of FUS function impair neuromuscular synaptic transmission in a genetic model of ALS. *Human molecular genetics* **22**, 4282–4292, doi:10.1093/hmg/ddt278 (2013).
24. Patten, S. A. *et al.* Neuroleptics as therapeutic compounds stabilizing neuromuscular transmission in amyotrophic lateral sclerosis. *JCI insight* **2**, doi:10.1172/jci.insight.97152 (2017).
25. Giacomotto, J., Rinkwitz, S. & Becker, T. S. Effective heritable gene knockdown in zebrafish using synthetic microRNAs. *Nature communications* **6**, 7378, doi:10.1038/ncomms8378 (2015).
26. 10.1155/2012/350352
    Leong, I. U., Lan, C. C., Skinner, J. R., Shelling, A. N. & Love, D. R. In vivo testing of microRNA-mediated gene knockdown in zebrafish. *Journal of biomedicine & biotechnology* 2012, 350352, doi:10.1155/2012/350352 (2012).
27. Kawakami, K., Shima, A. & Kawakami, N. Identification of a functional transposase of the Tol2 element, an Ac-like element from the Japanese medaka fish, and its transposition in the zebrafish germ lineage. *Proceedings of the National Academy of Sciences of the United States of America* **97**, 11403–11408, doi:10.1073/pnas.97.21.11403 (2000).

28. Shaw, M. P. *et al.* Stable transgenic C9orf72 zebrafish model key aspects of the ALS/FTD phenotype and reveal novel pathological features. *Acta neuropathologica communications* **6**, 125, doi:10.1186/s40478-018-0629-7 (2018).
29. Da Costa, M. M. *et al.* A new zebrafish model produced by TILLING of SOD1-related amyotrophic lateral sclerosis replicates key features of the disease and represents a tool for in vivo therapeutic screening. *Disease models & mechanisms* **7**, 73–81, doi:10.1242/dmm.012013 (2014).
30. Sakowski, S. A. *et al.* Neuromuscular effects of G93A-SOD1 expression in zebrafish. *Molecular neurodegeneration* **7**, 44, doi:10.1186/1750-1326-7-44 (2012).
31. Neumann, M. *et al.* Ubiquitinated TDP-43 in frontotemporal lobar degeneration and amyotrophic lateral sclerosis. *Science* **314**, 130–133, doi:10.1126/science.1134108 (2006).
32. Mori, F. *et al.* Phosphorylated TDP-43 aggregates in skeletal and cardiac muscle are a marker of myogenic degeneration in amyotrophic lateral sclerosis and various conditions. *Acta neuropathologica communications* **7**, 165, doi:10.1186/s40478-019-0824-1 (2019).
33. Schmid, B. *et al.* Loss of ALS-associated TDP-43 in zebrafish causes muscle degeneration, vascular dysfunction, and reduced motor neuron axon outgrowth. *Proceedings of the National Academy of Sciences of the United States of America* **110**, 4986–4991, doi:10.1073/pnas.1218311110 (2013).
34. Jensen, B. K. *et al.* Synaptic dysfunction induced by glycine-alanine dipeptides in C9orf72-ALS/FTD is rescued by SV2 replenishment. *EMBO molecular medicine* **12**, e10722, doi:10.15252/emmm.201910722 (2020).
35. Wei, C. *et al.* miR-153 regulates SNAP-25, synaptic transmission, and neuronal development. *PloS one* **8**, e57080, doi:10.1371/journal.pone.0057080 (2013).
36. Li, W., Ono, F. & Brehm, P. Optical measurements of presynaptic release in mutant zebrafish lacking postsynaptic receptors. *The Journal of neuroscience: the official journal of the Society for Neuroscience* **23**, 10467–10474 (2003).
37. Therrien, M., Rouleau, G. A., Dion, P. A. & Parker, J. A. Deletion of C9ORF72 results in motor neuron degeneration and stress sensitivity in C. elegans. *PloS one* **8**, e83450, doi:10.1371/journal.pone.0083450 (2013).
38. Ciura, S. *et al.* Loss of function of C9orf72 causes motor deficits in a zebrafish model of amyotrophic lateral sclerosis. *Annals of neurology* **74**, 180–187, doi:10.1002/ana.23946 (2013).
39. Atanasio, A. *et al.* C9orf72 ablation causes immune dysregulation characterized by leukocyte expansion, autoantibody production, and glomerulonephropathy in mice. *Scientific reports* **6**, 23204, doi:10.1038/srep23204 (2016).
40. Sudria-Lopez, E. *et al.* Full ablation of C9orf72 in mice causes immune system-related pathology and neoplastic events but no motor neuron defects. *Acta neuropathologica* **132**, 145–147, doi:10.1007/s00401-016-1581-x (2016).
41. Koppers, M. *et al.* C9orf72 ablation in mice does not cause motor neuron degeneration or motor deficits. *Annals of neurology* **78**, 426–438, doi:10.1002/ana.24453 (2015).

42. Swaminathan, A. *et al.* Expression of C9orf72-related dipeptides impairs motor function in a vertebrate model. *Human molecular genetics* **27**, 1754–1762, doi:10.1093/hmg/ddy083 (2018).
43. Swinnen, B. *et al.* A zebrafish model for C9orf72 ALS reveals RNA toxicity as a pathogenic mechanism. *Acta neuropathologica* **135**, 427–443, doi:10.1007/s00401-017-1796-5 (2018).
44. Ohki, Y. *et al.* Glycine-alanine dipeptide repeat protein contributes to toxicity in a zebrafish model of C9orf72 associated neurodegeneration. *Molecular neurodegeneration* **12**, 6, doi:10.1186/s13024-016-0146-8 (2017).
45. Lee, Y. B. *et al.* Hexanucleotide repeats in ALS/FTD form length-dependent RNA foci, sequester RNA binding proteins, and are neurotoxic. *Cell reports* **5**, 1178–1186, doi:10.1016/j.celrep.2013.10.049 (2013).
46. Zhu, Q. *et al.* Reduced C9ORF72 function exacerbates gain of toxicity from ALS/FTD-causing repeat expansion in C9orf72. *Nature neuroscience* **23**, 615–624, doi:10.1038/s41593-020-0619-5 (2020).
47. Custer, K. L., Austin, N. S., Sullivan, J. M. & Bajjalieh, S. M. Synaptic vesicle protein 2 enhances release probability at quiescent synapses. *The Journal of neuroscience: the official journal of the Society for Neuroscience* **26**, 1303–1313, doi:10.1523/JNEUROSCI.2699-05.2006 (2006).
48. Crowder, K. M. *et al.* Abnormal neurotransmission in mice lacking synaptic vesicle protein 2A (SV2A). *Proceedings of the National Academy of Sciences of the United States of America* **96**, 15268–15273, doi:10.1073/pnas.96.26.15268 (1999).
49. Yin, S. *et al.* Evidence that C9ORF72 Dipeptide Repeat Proteins Associate with U2 snRNP to Cause Mis-splicing in ALS/FTD Patients. *Cell reports* **19**, 2244–2256, doi:10.1016/j.celrep.2017.05.056 (2017).
50. Leenders, A. G., Lopes da Silva, F. H., Ghijsen, W. E. & Verhage, M. Rab3a is involved in transport of synaptic vesicles to the active zone in mouse brain nerve terminals. *Molecular biology of the cell* **12**, 3095–3102, doi:10.1091/mbc.12.10.3095 (2001).
51. Binotti, B., Jahn, R. & Chua, J. J. Functions of Rab Proteins at Presynaptic Sites. *Cells* **5**, doi:10.3390/cells5010007 (2016).
52. Mahoney, T. R. *et al.* Regulation of synaptic transmission by RAB-3 and RAB-27 in Caenorhabditis elegans. *Molecular biology of the cell* **17**, 2617–2625, doi:10.1091/mbc.E05-12-1170 (2006).
53. Ioannou, M. S. *et al.* DENND2B activates Rab13 at the leading edge of migrating cells and promotes metastatic behavior. *J Cell Biol* **208**, 629–648, doi:10.1083/jcb.201407068 (2015).
54. Allaire, P. D. *et al.* The Connecdenn DENN domain: a GEF for Rab35 mediating cargo-specific exit from early endosomes. *Molecular cell* **37**, 370–382, doi:10.1016/j.molcel.2009.12.037 (2010).
55. Westerfield, M. *The zebrafish book: a guide for the laboratory use of zebrafish (Brachydanio rerio)*. (M. Westerfield, 1993).
56. Kimmel, C. B., Ballard, W. W., Kimmel, S. R., Ullmann, B. & Schilling, T. F. Stages of embryonic development of the zebrafish. *Developmental dynamics: an official publication of the American Association of Anatomists* **203**, 253–310, doi:10.1002/aja.1002030302 (1995).

Figures

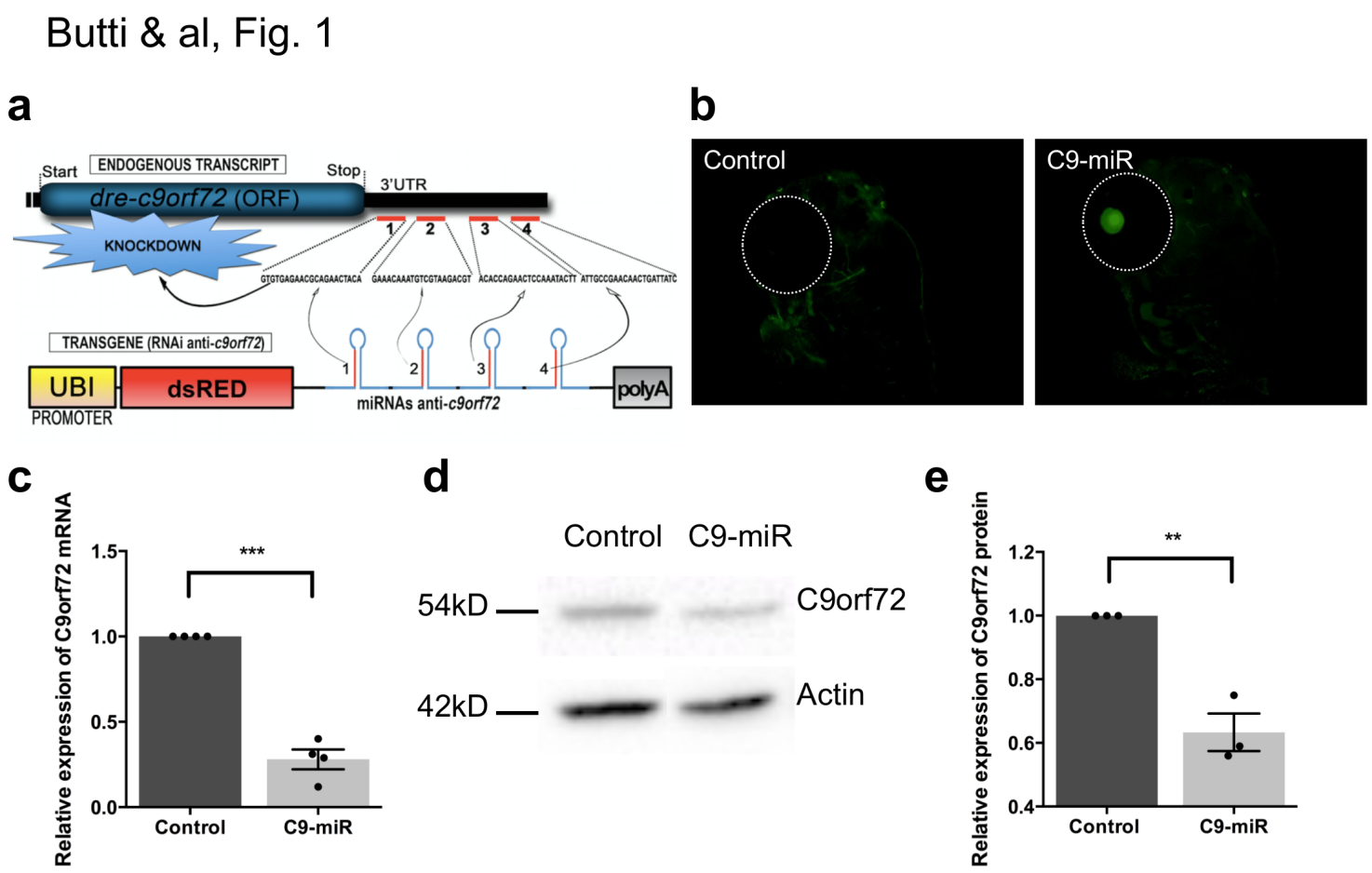

Figure 1

Generation of a stable zebrafish C9orf72 knockdown line. a. Schematic representation of the technique use to silence C9orf72 in zebrafish. The transgene is designed to express four different micro-RNAs targeting C9orf72' 3'UTR and triggering knockdown by both repressing C9orf72 translation and affecting its stability. b. Snapshot demonstrating proper eGFP expression in the crystallin of the transgenic fish, a marker used to identify carrier/knockdown larvae. c. Histogram shows the relative expression of the endogenous C9orf72 gene. mRNA was normalized to elf1α mRNA levels (n=4, p value<0.0001). d. Immunoblotting of the Zebrafish protein C9orf72 and actin as control. e. Histogram shows the relative expression of the C9orf72 protein compared with actin between C9orf72 mutants and control line (n=3, p value=0.0034). *** denotes p<0.0001; ** denotes p<0.005. Data are presented as mean±SEM.

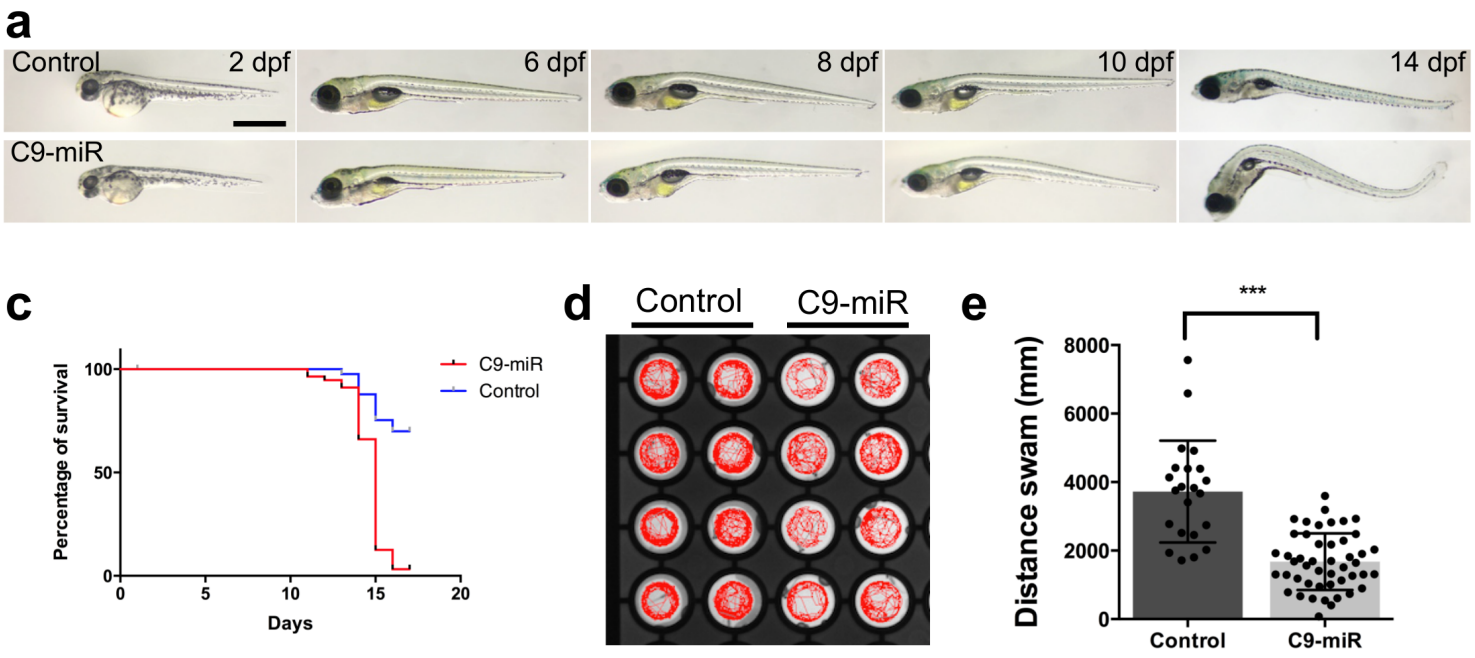

Figure 2

Characterization of zebrafish C9orf72 LOF line. a. Representative images of the C9orf72 LOF line (C9-miR) compared to control line during larval development showing great morphological defects. b. Kaplan curves over 17 days showing low survival rate in C9-miR compared to controls. c. Schematic representation of each zebrafish larval movement at 6 dpf fish. d. C9-miR larvae displayed impaired swimming compared to controls (N=3, n=21-48). Data are presented as mean±SEM. *** denotes $p<0.0001$.

Butti & al, Fig. 3

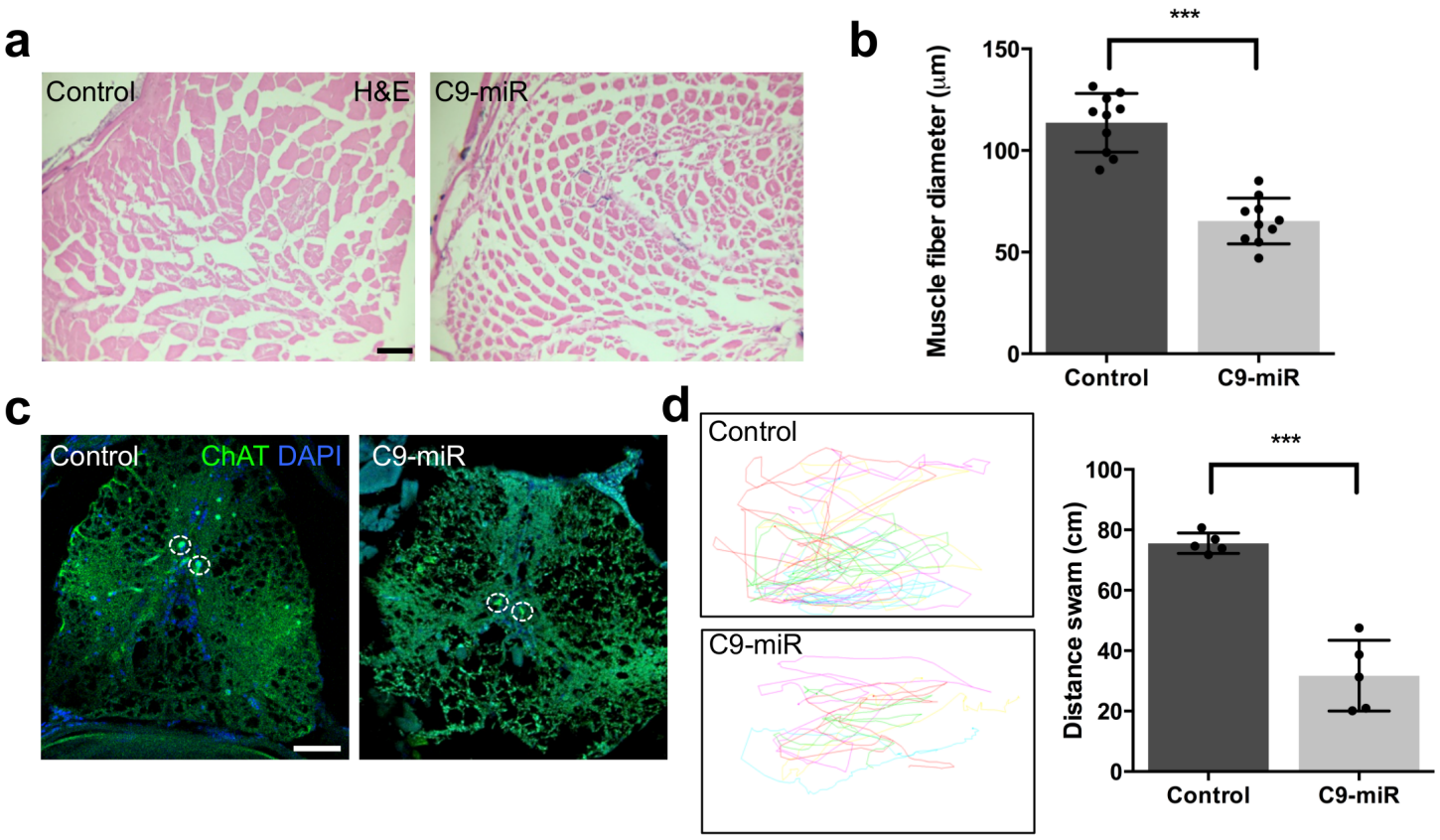

Figure 3

Adult zebrafish C9-miR display muscle atrophy, smaller motoneurons and behavioural deficits. a. Representative Hematoxylin and Eosin staining of adult zebrafish muscle myotomes. b. C9-miR fish display a smaller diameter of muscle fibres compared to controls (N=10; p value<0.0001). c. ChAT staining in adult zebrafish spinal cord. Large motor neurons (broken circle) are reduced in size in C9-miR compared to controls. d. Representative traces of swimming activity of five adults control and C9-miR fishes during thirty seconds (left panel). C9-miR fish exhibit behavioural deficits (right panel). Data are presented as mean±SEM. *** denotes p<0.0001. Scale bar = 50 M.

Butti & al, Fig. 4

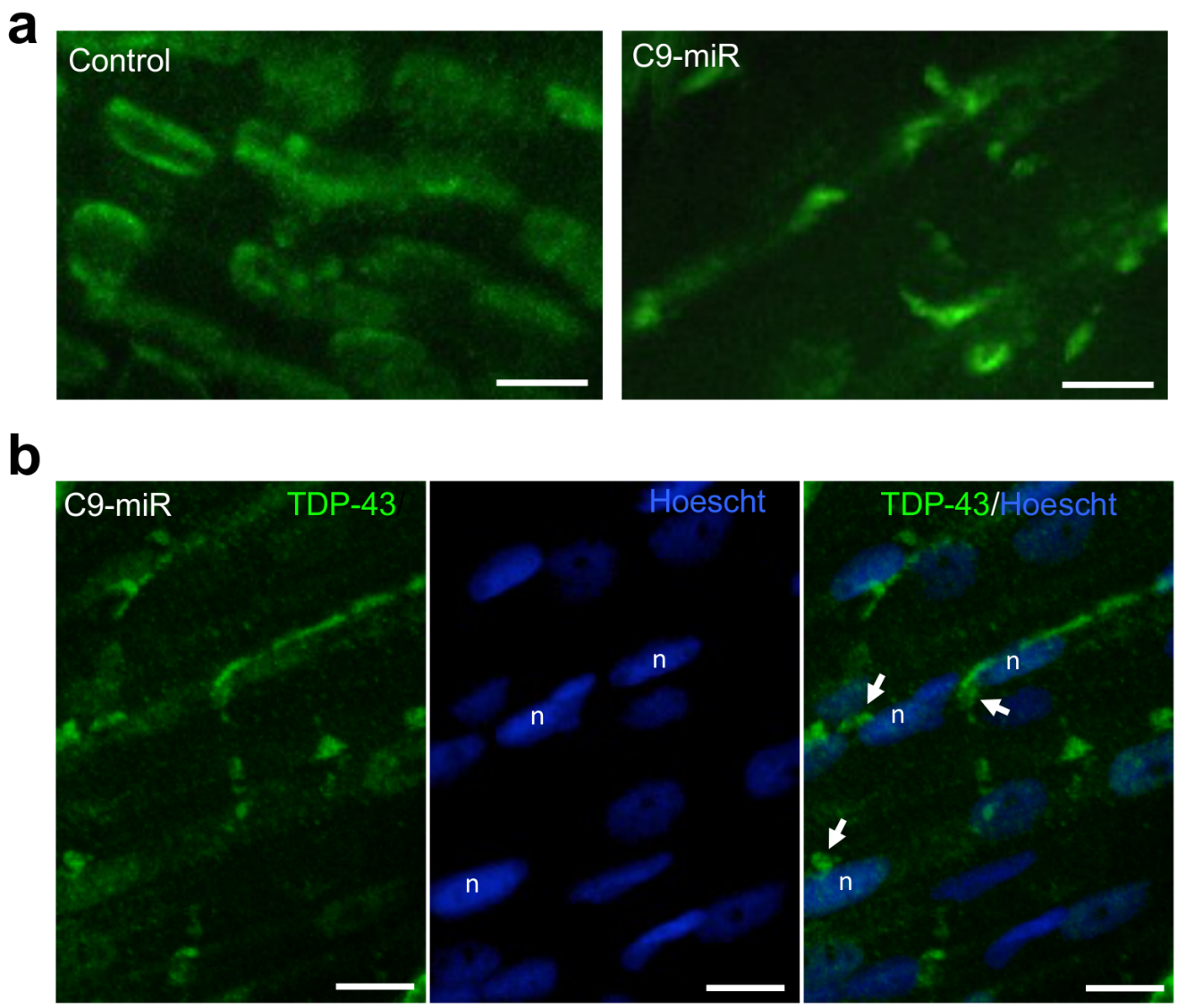

Figure 4

Zebrafish C9-miR displayed TDP-43 pathology. a. Representative images of 6dpf zebrafish skeletal muscle cells labelled for TDP-43. Compared to controls fish, we observed clustering of TDP-43 expression in C9-miR skeletal muscles. b. TDP-43 is mislocalization outside of the nucleus in C9-miR zebrafish. Scale bar = 10 µM ; N=5 ; Arrows indicate clusters of TDP-43 expression ; n : nucleus.

Butti & al, Fig. 5

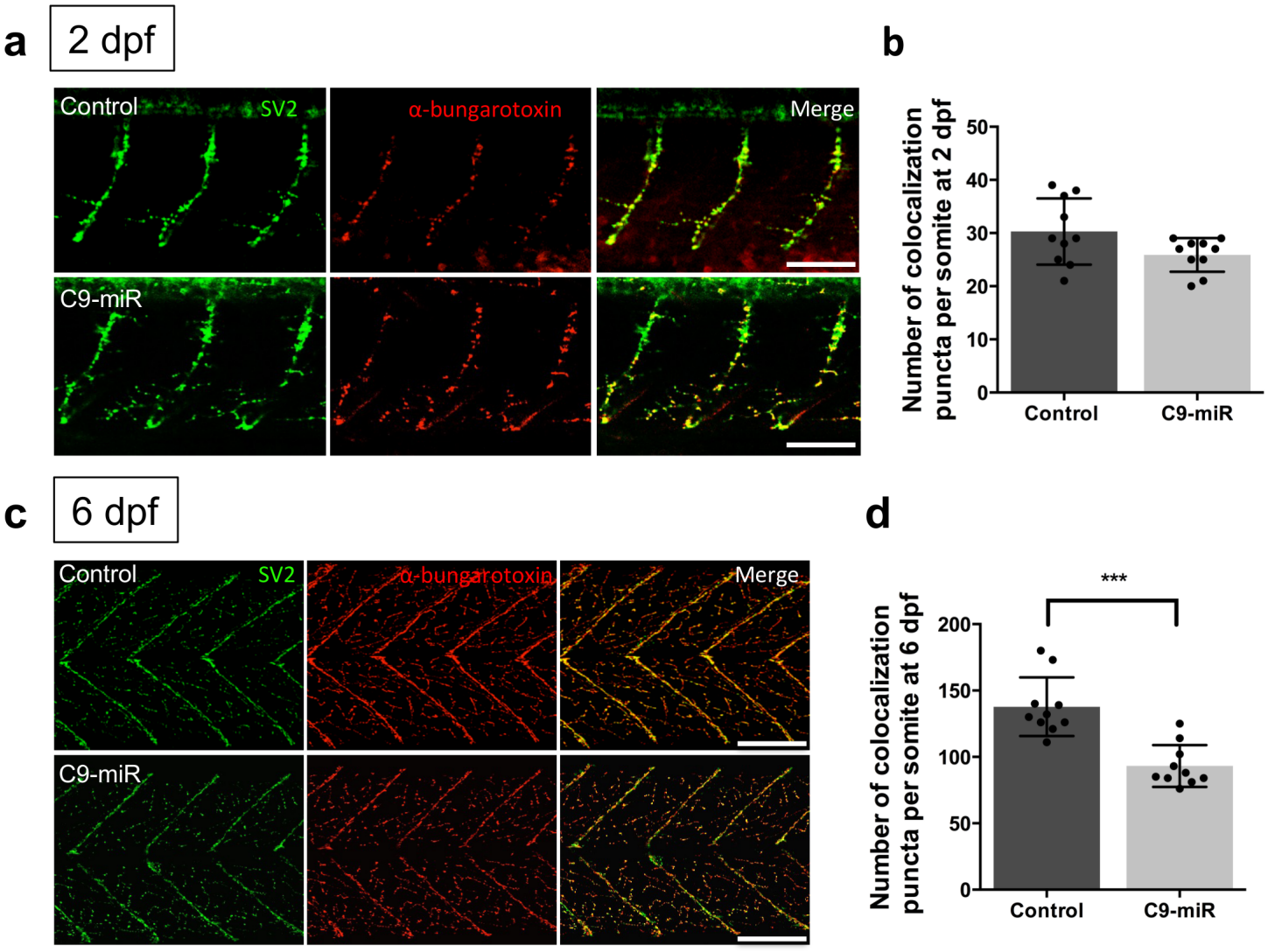

Figure 5

Zebrafish C9-miR displayed reduced acetylcholine receptor clusters at neuromuscular junctions. a. Representative images of co-immunostaining of zebrafish neuromuscular junctions with presynaptic (SV2a) and postsynaptic (α-bungarotoxin) markers in 2dpf zebrafish. Scale bar = 50 M. b. Quantification of the colocalizing pre-and post-synaptic markers per somite showed no differences between C9-miR and controls at early embryonic stages (2 dpf; N=8; p value =0.064). c. Representative images of co-immunostaining of zebrafish neuromuscular junctions with SV2a and α-bungarotoxin in 6dpf zebrafish. Scale bar = 100 M. d. Quantification of the colocalizing pre-and post-synaptic markers per somite showed a significant reduction in puncta in C9-miR fish at late larval stages embryonic stages (6 dpf; N=8). *** denotes p<0.0001.

Butti & al, Fig. 6

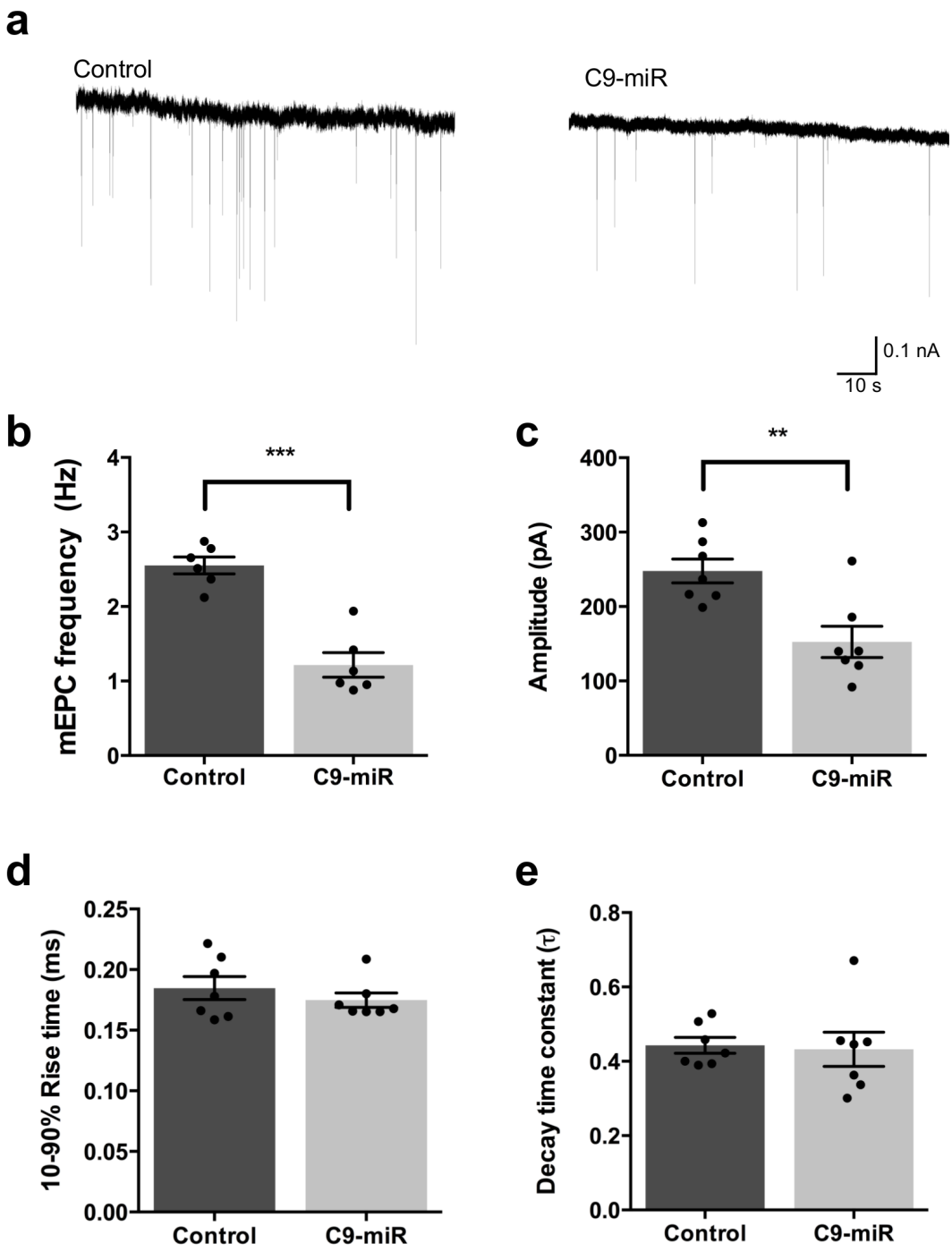

Figure 6

Zebrafish C9-miR exhibited attenuated miniature endplate currents (mEPCs) at NMJs. a. Recordings of mEPCs, which result from spontaneous release of a quantum, were recorded in 6dpf controls and C9-miR. Animals with reduced C9orf72 (C9-miR) displayed mEPCs with reduced frequency (b) and amplitude (c). Rise time (d) and decay time (e) constant kinetics of mEPC was not found to be significantly different. N=7; *** denotes p<0.0001.

Butti & al, Fig. 7

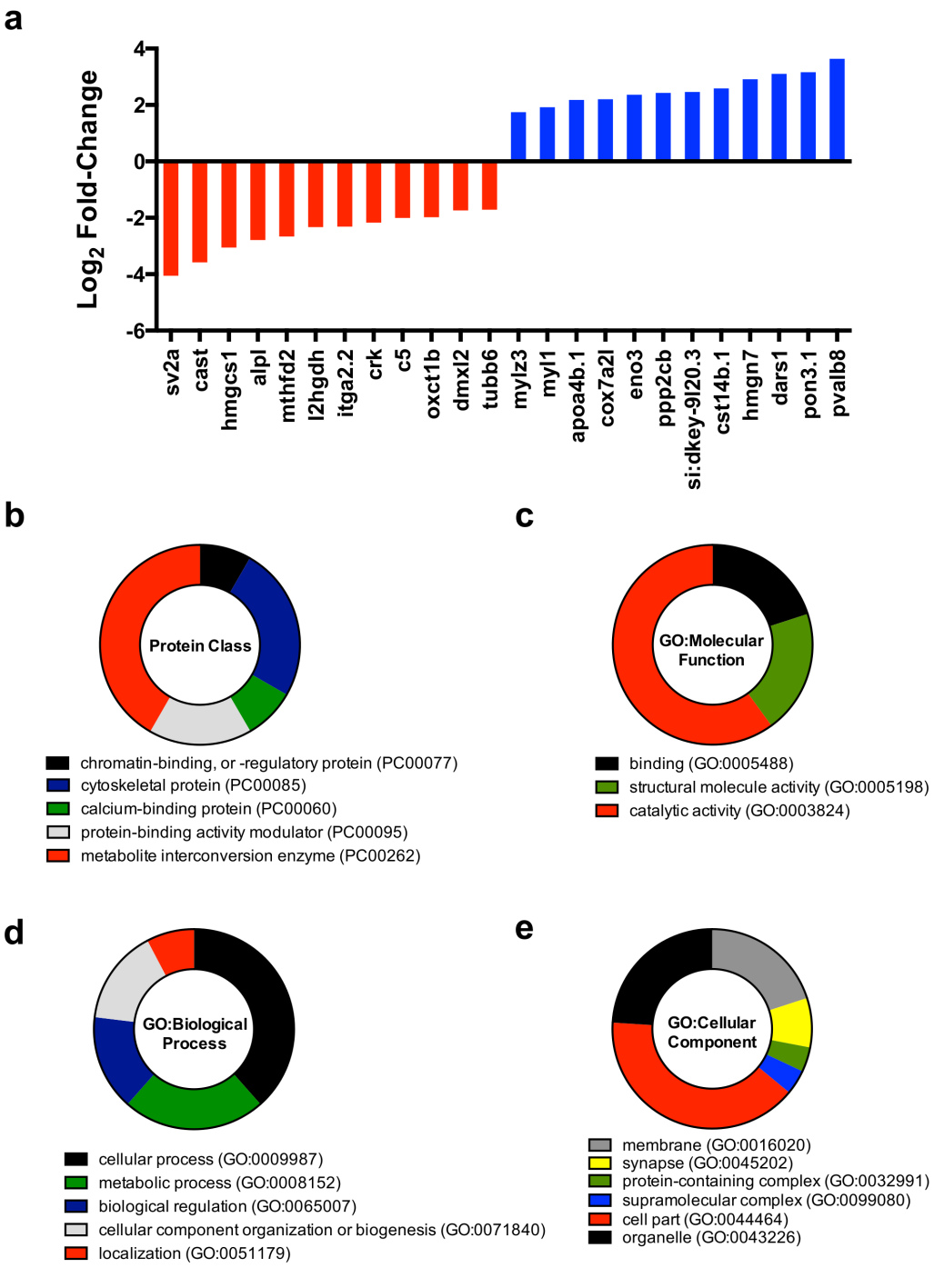

Figure 7

Proteomic analysis in C9-miR and control larvae. a. Differentially expressed proteins with $p<0.05$ in C9-miR larvae. Protein Class (b), Molecular function (c), Biological processes (d) and Cell component (e) GO-term classifications that are enriched in the differentially expressed proteins.

Butti & al, Fig. 8

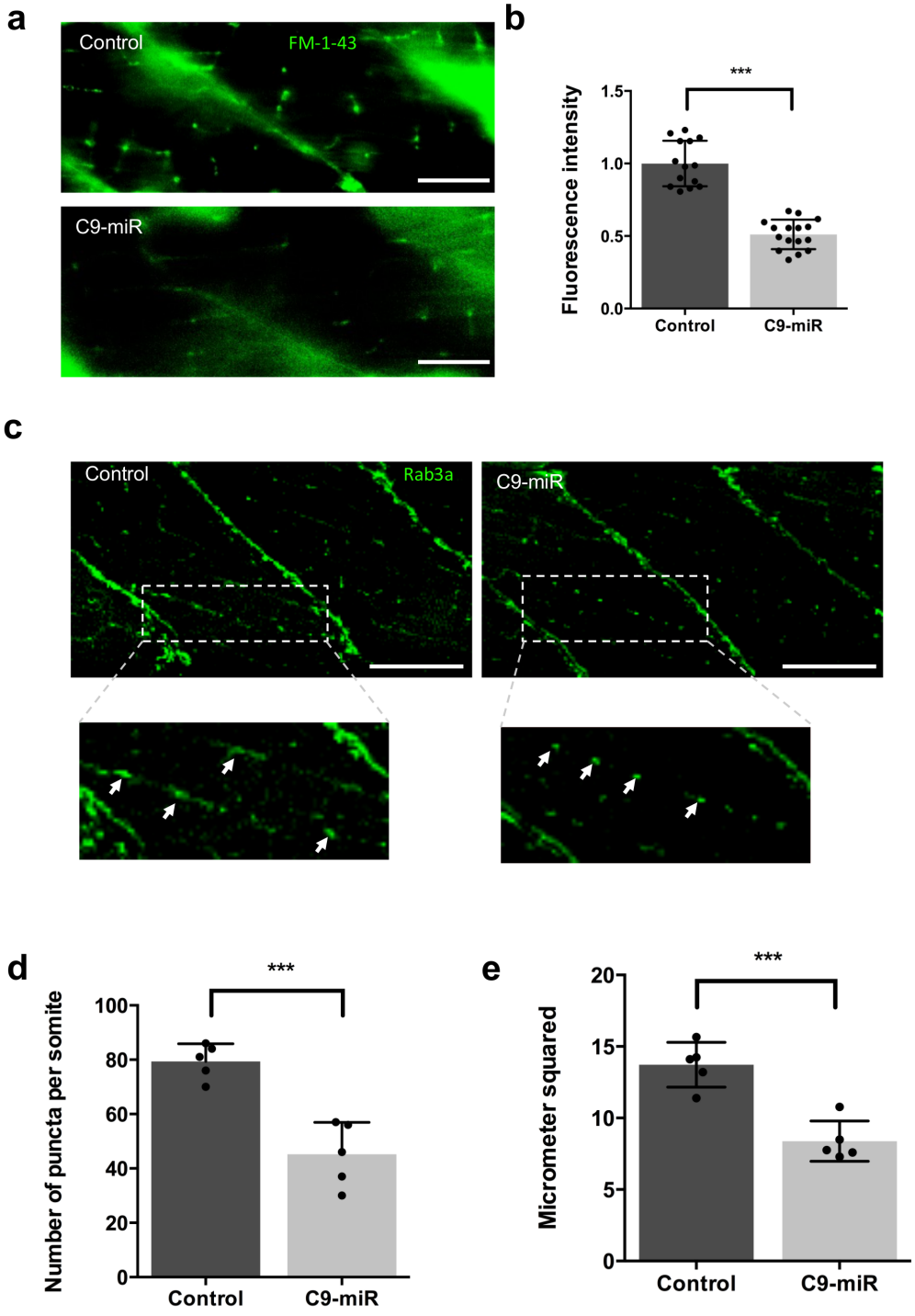

Figure 8

C9orf72 regulates synaptic active zones and activity at the neuromuscular junction. a. FM1-43 loading of NMJ boutons in 6 dpf fish. C9-miR displayed decreased FM1-43 loading. b. Quantification of FM1-43 fluorescent intensity in control and C9-miR fish. c. Putative synapses (arrows) were visualized with Rab3a immunostaining at 6 dpf. Rab3a+-synaptic puncta were reduced in number (d) and area (e) in 6 dpf C9-miR larvae when compared with wild-type controls (N=5). Scale bar = 50 M.*** denotes p<0.0001.

Supplementary Files

This is a list of supplementary files associated with this preprint. Click to download.

- FigS1.tif
- WTadult.avi
- C9mutadult.avi